Thermodynamic Behavior of Poly(3-alkyl Thiophene) Blends: Equilibrium Cocrystal Formation and Phase Segregation

Susmita Pal and Arun K. Nandi*

Polymer Science Unit, Indian Association for the Cultivation of Science, Jadavpur, Kolkata-700032, India

Received: August 26, 2004; In Final Form: December 13, 2004

The equilibrium cocrystal formation of poly(3-alkyl thiophene) (P3AT) blends has been studied by isothermal cocrystallization in a differential scanning calorimeter (DSC-7). The equilibrium melting points (T_m^0) of the cocrystals are measured using the Hoffman−Weeks extrapolation procedure. The equilibrium phase diagrams are of three different types: (a) concave upward, (b) linear, and (c) linear with phase separation at higher content of lower melting component. The phase diagram nature depends on the regioregularity difference and also on the difference in the number of carbon atoms in the pendent alkyl group of the components. The origin of biphasic nature of type "c" phase diagram has been explored from the glass transition temperature (T_g) measurement using a dynamic mechanical analyzer. The biphasic compositions show two glass transition temperatures (T_g) as well as two β transition temperatures (T_β). The T_gs of phase-separated regions correspond to almost the component values but the T_βs correspond to that of a lower (T_β) component value, and the other is higher than that of the higher (T_β) component value. Possible reasons are discussed from the interchain lamella thickness in the P3AT blends and molecular modeling using molecular mechanics program.

Introduction

Poly(3-alkyl thiophenes) (P3ATs) produce cocrystals under quenched states from the melt.[1] The cocrystallization is limited to the pendent alkyl chain length difference of two carbon atoms and is also limited to the head−tail (H−T) regioregularity difference of 17 mol %. Besides, the cocrystallization is also specific to the composition of the blend in some systems. So it is important to study whether the P3ATs produce equilibrium cocrystals and to elucidate the reasons for the difference in cocrystallization behavior for varying blend compositions of some systems. In this paper, we present a study on the formation of equilibrium cocrystals from the thermodynamic behavior of isothermal crystallization of the blends. We also present a dynamic mechanical property study of the cocrystals of different composition to elucidate the cause of biphasic nature at certain compositions of some blends.

The thermodynamic study of cocrystallization is an important tool to help understand the cocrystallization process, and in the literature, few reports exist at this end.[2−11] The most important condition of cocrystallization is that the component polymers should be miscible in the melting state.[5,6] The phase diagrams of crystalline polymers miscible in the melting state exhibit four different behaviors: (I) immiscible with eutectic; (II) immiscible with no eutectic; (III) miscible with concave upward (weak interaction); (IV) miscible with concave downward (strong interaction).[2] Tanaka et al. studied the phase diagram of vinylidene fluoride−trifluoro ethylene (VF_2−F_3E) copolymers and observed type II and type III natures of the phase diagram depending on the copolymer composition of the components[2]. Keller and co-workers observed that the cocrystals of linear polyethylene and branched polyethylene are biphasic in nature at certain compositions and attributed it to the liquid−liquid-phase separation of the melting state at those compositions.[4] However, Alamo et al. concluded from neutron-scattering study that the phase segregation in this system is due to the crystallization process.[7] Similar controversial report of cocrystallization is also found for poly(vinyl fluoride) (PVF) and a poly(vinylidene fluoride) system.[3,5] The controversial reports might arise from the use of different samples and also of different crystallization conditions for cocrystallization by different workers. Kamiya et al. studied the phase diagram of copolymers of 3-hydroxylbutyrate and 3-hydroxy valerate (p(3HB−3HV)) system[10] and Jeong et al. studied the phase diagram of poly(butylene terephthalate-*co*-butelene-2,6-naphthalate) system.[11] Both systems exhibit isodimorphic character in their phase diagrams. We recently studied the phase diagram of poly(vinylidene fluoride) (PVF_2) and vinylidene fluoride−tetrafluoro ethylene (VF_2−VF_4) copolymers[6] and observed type III, linear, and coexisting concave upward and concave downward curves depending on the head to head (H−H) defect/(VF_2−VF_4) co-unit content in the chains of the components. The linear plot indicates ideal mixing of the components, while the coexisting concave upward and downward curve indicates immiscibility both in the melt and in the solid state.[12]

P3ATs are important conducting polymers for their excellent electrical conductivity, electroluminescence property, nonlinear optical properties, etc. and find uses in various electronic and optoelectronic applications.[13] They are comblike polymers and have an interchain lamellar structure in the solid state; the lamellar distance depends on the length of the alkyl groups.[1,14,15] The formation of the cocrystal is characterized by formation of single lamella with intermediate interchain lamellar distance. Again the X-ray patterns of the cocrystals produced under the melt-state quenched condition indicate the formation of type I crystals i.e., interdigition of side chains, is minimal[15] in the lamella. The cocrystals have either intermediate or lower conductivity than the arithmetic average of their component values.[1] The phase diagrams drawn from the melting points of melt-quenched samples exhibit a different nature depending on

* Author to whom correspondence may be addressed. E-mail: psuakn@mahendra.iacs.res.in.

10.1021/jp046148c CCC: $30.25
Published on Web 01/28/2005

TABLE 1: Characteristics of the Samples Used in the Work

P3AT samples	source	$\overline{M_W} \times 10^4$	HT regioregularity (mol %)	Mp[a] (°C)
P3HT(R)	Aldrich Chem.Co.	8.7	92	222
P3OT(R)	Aldrich Chem. Co.	14.2	89	164
P3HT-1	prepared	8.7	75	161
P3HT-2	prepared	10.6	82	182

[a] Melting points of melt-quenched (at −30 °C) samples at the heating rate of 20°/min.

the amount of regioregularity and side-chain length. In most cases, the phase diagrams are linear but biphasic regions at lower melting components reach regions of the regioregular poly(3-octyl thiophene) (P3OT-(R))/regioregular poly(3-hexyl thiophene) (P3HT-(R)) system, and the regioregular poly(3-hexyl thiophene) (P3HT-(R))/regioirregular poly(3-hexyl thiophene) (P3HT-1) system is also observed. The aim of this work is to judge whether the biphasic nature is an equilibrium phenomenon and what is the cause of this different behavior than the other compositions of the same system. Also the phase diagrams based on equilibrium melting point have been presented as they may give an insight to the thermodynamic nature of the cocrystals and also to their melt.[2,6] The equilibrium melting points of the cocrystals have been determined from isothermal crystalization at different isothermal temperatures. And the origin of the biphasic nature has been elucidated from the T_g measurement of melt-quenched samples using dynamic mechanical property measurement. This study is also important from the technological point of view as it may dictate the use of the cocrystals for a wide temperature range.

Experimental Section

The P3AT samples were prepared as mentioned earlier,[16] and the regioregular samples were purchased from Aldrich Chemical Co., U.S.A. The characteristics of the samples are presented in Table 1. Cocrystals were prepared by making solvent-cast films from the solution of two component polymers in different weight ratios in distilled chloroform and then drying in a vacuum at 60 °C for 3 days.[1]

Isothermal crystallization of the samples was performed taking 5 mg of the above samples in aluminum pans. They were melted in a differential scanning calorimeter (DSC-7, Perkin-Elmer) at 250 and 220 °C for five minutes for P3HT(R) blends and for the other blends, respectively. They were then quenched in the DSC at the rate of 200 °C/min from the melting temperature to the predetermined isothermal temperature (T_c), at which point they were crystallized for different times. The samples were heated from the T_c at the heating rate of 10 °C/min without cooling. The melting point and enthalpy of fusion of the samples were measured from the endotherm using a computer attached to the instrument. The instrument was operated under nitrogen atmosphere and calibrated with indium before each set of experiments. Representative melting thermograms of the P3HT-2/P3OT(R) blend ($W_{P3OT(R)} = 0.75$) are shown in Figure 1 for crystallization at 138 °C for different times. The melting peaks are broad, but no component melting peaks (Table 1) are observed, indicating cocrystal formation at this isothermal condition.

For the measurement of T_g of some blends by use of the dynamic mechanical analyzer (DMA), the films (25 mm × 5 mm × 0.15 mm) of the blends were cast in a dice and dried in a vacuum for 3 days. They were melted in a Mettler FP 82 hot-stage at the temperatures as mentioned above under nitrogen

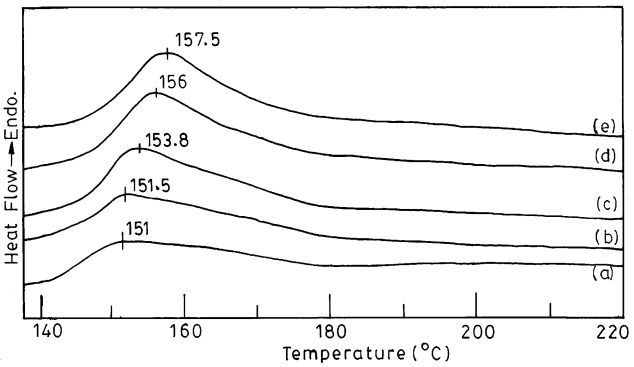

Figure 1. Representative DSC thermograms showing the melting of a P3HT-2/P3OT(R) blend ($W_{P3OT(R)} = 0.75$) for isothermal crystallization at 138 °C for predetermined times: (a) 5 min, (b) 15 min, (c) 60 min, (d) 3 h, and (e) 5 h (at heating rate 10°/min).

atmosphere and quenched to −30 °C in a thermostatic bath to produce the cocrystals under the melt-quenched condition. The films were then installed in the tension clamp of the calibrated DMA instrument (TA instruments, model Q-800). The samples were heated from −130 to 100 °C at a heating rate of 10°/ min. The instrument was operated at a constant frequency of 10 Hz with a static force of 0.02 N. Approximate models of the P3AT cocrystals are made using a molecular mechanics (MMX) program.[17] The P3AT structures were drawn and moved to each other for predetermined lamella thickness, and then energy minimization was done. The distances are then enquired using the program and are shown in the figure.

Results and Discussion

(a) Equilibrium Phase Diagram. To measure the equilibrium melting temperature of cocrystals, the Hoffman−Weeks extrapolation method[18,19] has been adopted according to the following equation

$$T_m = T_m^0\left(1 - \frac{1}{\gamma}\right) + \frac{T_c}{\gamma} \qquad (1)$$

where T_m is the apparent melting point of the sample crystallized at the crystallization temperature (T_c) and γ is the thickening ratio. Determination of correct T_m at a given T_c for the Hoffman−Weeks plot is difficult, and care should be taken to monitor the correct T_m at a given T_c.[20] It is now established that the melting point of very low and same level of crystallinity at each T_c yields accurate T_m^0 values by this method.[21,22] In this case, we adopted the melting point of the crystals having an enthalpy of fusion of 2 J/g as in the blends the ΔH_u^0 (enthalpy of fusion of perfect crystal) which may vary with composition to yield the actual value of crystallinity is not known. This is because P3OT(R) and P3HT(R) have different ΔH_u^0 values,[23] and again it may also vary with regioregularity of the samples.[21] In Figure 2 , a representative plot of T_m against enthalpy is shown for different T_c values for the blend P3HT-2/P3OT(R) of composition $W_{P3OT(R)} = 0.75$. It is apparent from the figure that initially the melting point remains constant, but at higher enthalpy values, the T_m increases probably due to the thickening process. With an increase in T_c, the thickening starts at lower enthalpy values than that at lower T_c values. In Figure 3, the melting point of the samples having enthalpy values of 2 J/g are plotted for each T_c for the P3OT(R)/P3HT-2 blends. All the data, when extrapolated, meet at the $T_m = T_c$ line, and the intersection point yields the T_m^0 value. The uncertainty in the extrapolation values is ±2 °C. The $T_m - T_c$ plots of the

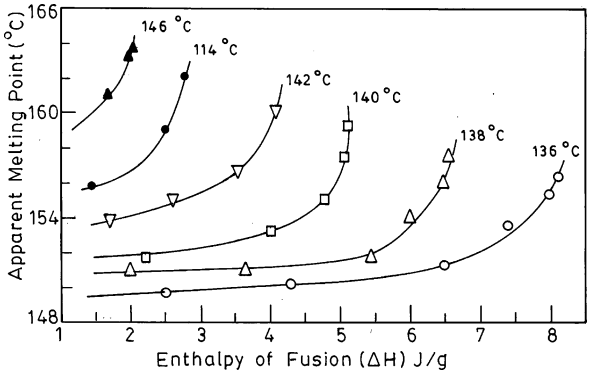

Figure 2. A representative plot of apparent melting points against enthalpy of fusion of the P3HT-2/P3OT(R) blend ($W_{P3OT(R)} = 0.75$) at indicated isothermal crystallization temperatures (T_c).

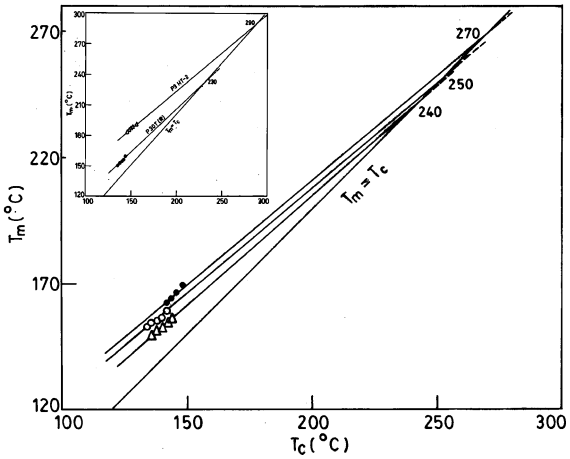

Figure 3. Hoffman−Weeks plot of P3HT-2/P3OT(R) blends (T_m is taken for enthalpy of fusion of 2 J/g at each T_c). (△) $W_{P3OT(R)} = 0.75$, (○) $W_{P3OT(R)} = 0.5$, (●) $W_{P3OT(R)} = 0.25$. Inset: Hoffman−Weeks plot of P3HT-2 and P3OT(R).

components are shown in the inset of the Figure 3, and it is apparent from the figure that the T_m^0 values of the blends are intermediate of the component values.

A different situation occurs for the P3HT(R)/P3OT(R) and P3HT(R)/P3HT-1 blends at lower melting component rich regions. Here two melting peaks are observed for the isothermally crystallized samples as observed in the melt quenched samples.[1] A representative figure for the P3HT(R)/P3HT-1 system ($W_{P3HT-1} = 0.75$) is shown in Figure 4. It is apparent from the figure that there are two melting peaks whose size increases with increasing crystallization time. The higher melting peak, however, decreased to some extent with increasing crystallization time, indicating this phase has some irregular chains which are gradually incorporated into the crystalline lattice of regioregular chains.[24] Hoffman−Weeks plots are made for each peak as earlier and are shown in Figure 5. It clearly indicates that there are two equilibrium melting points, which are not exactly identical with those of the parent components.

In Figure 6, the T_m^0 values are plotted with composition of the blends to obtain the equilibrium phase diagram. From the results, the equilibrium phase diagrams can be categorized into three different types: (i) P3HT-1/P3HT-2 and P3HT(R)/P3HT-2 blends show a linear plot indicating ideal mixing, (ii) the P3OT(R)/P3HT-2 system exhibits a concave upward curve indicating weak interaction between the components, and (iii) P3HT(R)/P3HT-1 and P3HT(R)/P3OT(R) systems exhibit a

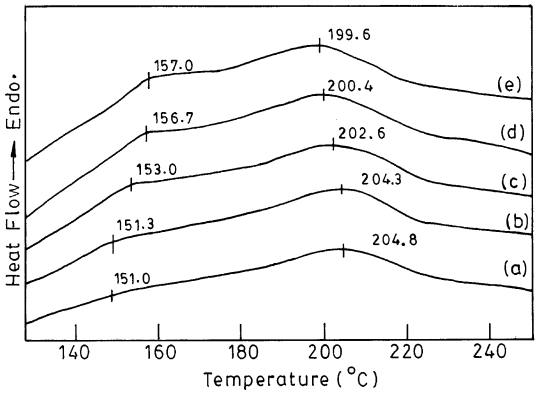

Figure 4. Representative DSC thermograms of a phase-separated P3HT(R)/P3HT-1 blend ($W_{P3HT-1} = 0.75$) for isothermal crystallization at 132 °C for different crystallization times: (a) 5 min, (b) 15 min, (c) 60 min, (d) 3 h, (e) 7 h (at heating rate 10°/min).

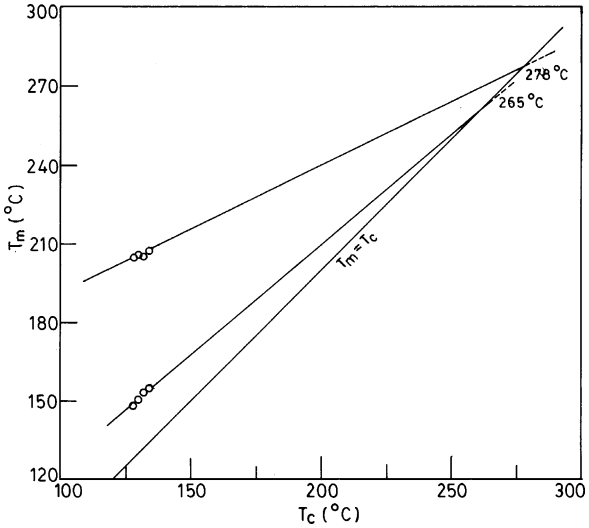

Figure 5. Hoffman−Weeks plots of a phase-separated P3HT(R)/P3HT-1 blend ($W_{P3HT-1} = 0.75$).

closed-loop phase diagram indicating the biphasic nature of the blends.[2,6] To elucidate the reason for the different nature of the phase diagrams, the difference in regioregularity, chain length difference of pendent groups, and molecular weight difference should be considered. The last contribution may be neglected, as molecular weight difference is not too large for the pairs studied here and also the molecular weight effect on the polymer−polymer interaction is negligible.[12] So, the regioregularity and pendent chain length differences should be taken into account to explain the phase diagram.

In the P3HT(R)/P3HT-2 and P3HT-1/P3HT-2 systems, the components differ in regioregularity and so also for P3HT(R)/P3HT-1 system. The former two pairs show ideal mixing as the difference of regioregularity is low, e.g., 10% for the first pair and 7% for the second pair. For the P3HT(R)/P3HT-1 system, the regioregularity difference is 17% and does not exhibit equilibrium cocrystallization at the whole composition range. The cause for the closed loop structure of the phase diagram of this system will be discussed later.

Now the equilibrium phase diagram of P3HT(R)/P3OT(R) and P3OT(R)/P3HT-2 systems will be compared. In the two systems, there is a variation of side chain length between the components by two carbon atoms, and there is a difference of regioregularity between the P3HT components. In the P3OT(R)/P3HT-2 system, the concave upward phase diagram

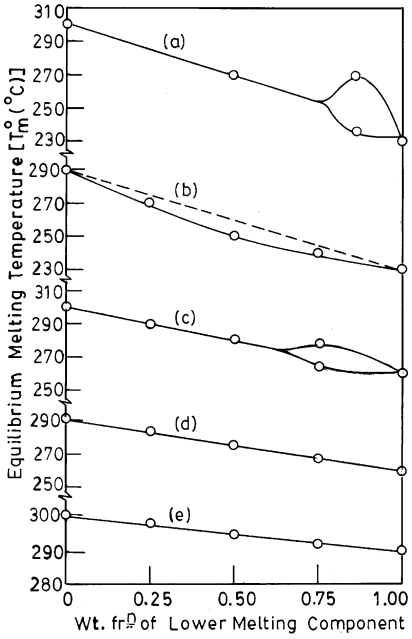

Figure 6. Equilibrium phase diagram of P3AT cocrystals. (a) P3HT-(R)/P3OT(R); (b) P3OT(R)/P3HT-2; (c) P3HT(R)/P3HT-1; (d) P3HT-1/P3HT-2; (e) P3HT(R)/P3HT-2 blends. The dashed line in (b) joins the component values.

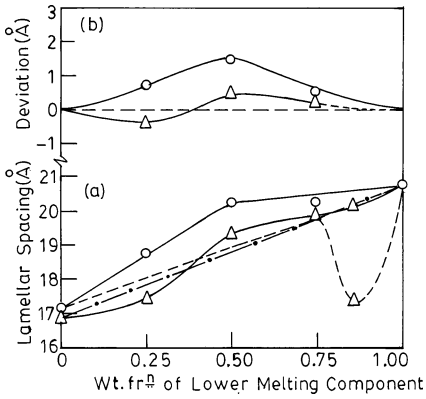

Figure 7. (a) Plot of interchain lamellar spacing vs weight fraction of lower melting components: (○) P3OT(R)/P3HT-2 and (△) P3HT(R)/P3OT(R). Dashed and dot-dashed lines are connecting the lines of component values. (Data are taken from Figures 8 and 10 of ref 1.) (b) Plot of lamellar spacing deviation (from the corresponding dashed and dot-dashed lines) vs weight fraction of lower melting components of the above blends. (The dashed line indicates zero deviation.).

indicates that there is a weak interaction between the components.[2] Probably, it may arise from the dispersion interaction of the overlapping hexyl and octyl side chains of the cocrystal lamella. But this is absent in the P3HT(R)/P3OT(R) system, probably because the regioregular P3HT(R) chain prefers to remain in a particular orientation and interdigitation of hexyl with octyl groups of P3OT(R) is not as favorable as that in P3HT-2. The P3HT-2 chain, because of its lesser regioregularity, can easily orient to intercalate the octyl chains of P3OT(R). A possible support for this assertion may be obtained from the lamellar thickness data obtained from wide-angle X-ray scattering data (WAXS) of ref 1 on the melt-quenched samples (Figure 7a). The P3OT(R)/P3HT-2 system shows a sharp increase of lamellar thickness and then a gradual increase with increasing P3OT(R). By consideration of an ideal increase in lamellar thickness, a dashed line is drawn, joining that of the components, and a positive deviation is observed. It probably

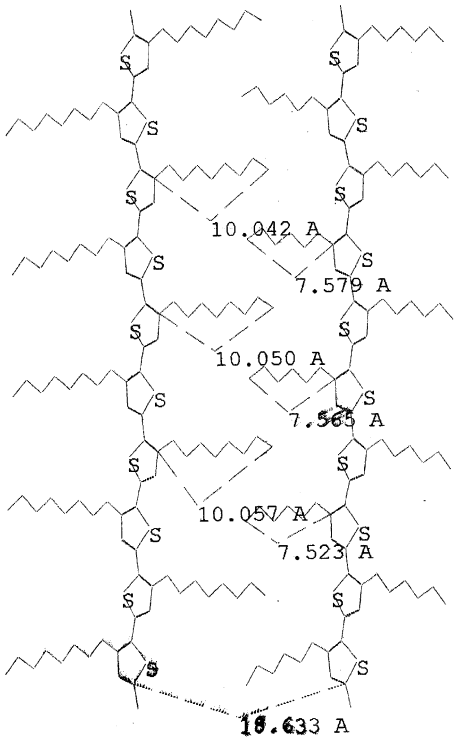

Figure 8. An approximate molecular model (energy minimized) of P3HT/P3OT system.

indicates that the hexyl and octyl groups are in extended-chain configurations so that there may be an overlap between the hexyl and octyl groups. This overlap yields a weak dispersion interaction in the blend. The deviations are plotted in Figure 7b, and it shows a maximum for the 50% composition. This is not true for the P3HT(R)/P3OT(R) system where the lamellar thickness vs composition plot is S-shaped and then bifurcated. The deviation is negative at the low P3OT(R) content blends, and it may arise because the side chains get squeezed while mixing with the P3HT(R). Such an arrangement of the pendent group decreases the dispersion interaction. To understand the above phenomena, an approximate molecular model of P3HT/P3OT system (energy minimized) is shown in Figure 8 having the lamellar thickness of 18.63 Å. The side-chain distances are longest at this lamellar thickness, but they decrease for both increasing and decreasing lamellar thickness (Table 2, Supporting Information). The longer the side chain length, the larger the dispersion interaction as interdigitation is larger. At the blend composition $W_{P3OT(R)} = 0.86$, two lamellar distances corresponding to the lamellar thickness of pure components are observed (Figure 8 of ref 1). This causes a bifurcation in the plot signifying non-cocrystallization at this composition.

(b) Phase Segregation. To elucidate the cause of the biphasic nature of the phase diagram at certain compositions of P3HT(R)/P3OT(R) and P3HT(R)/P3HT-1 blends, we measured the glass transition temperature (T_g) of some blends using the DMA. In Figures 9 and 10, the loss modulus plots of blends of P3HT(R)/P3OT(R) and P3HT(R)/P3HT-1 systems are shown. The loss modulus exhibits two peaks for the pure components. The higher-temperature peak of P3HT(R) at 20.3 °C is due to the glass transition, and the lower temperature peak at −101.2 °C is due to the β transition, i.e., for the onset of side-chain-relaxation process.[25] For P3OT(R), the T_g is at −9.2 °C, and the β transition temperature (T_β) is at −92.2 °C. So with increase in side-chain length, the glass transition temperature decreased. The increase in side-chain length makes the P3OT(R) structure

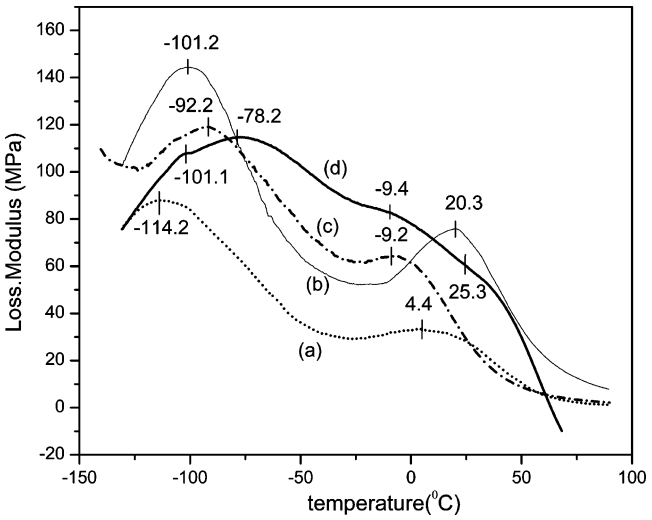

Figure 9. Loss modulus vs temperature plot (heating rate 10 °C/min) of melt-quenched P3HT(R)/P3OT(R) blends: (a) $W_{P3OT(R)} = 0.20$; (b) P3HT(R); (c) P3OT(R); (d) $W_{P3OT(R)} = 0.86$.

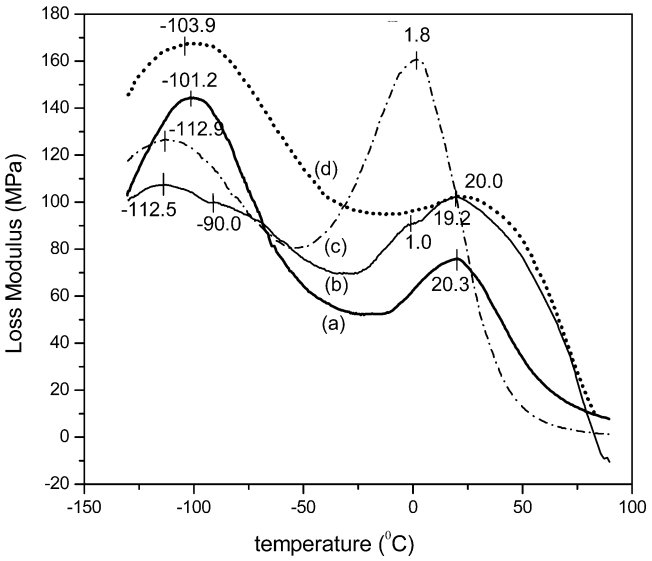

Figure 10. Loss modulus vs temperature plot (heating rate 10 °C/min) of melt-quenched P3HT(R)/P3HT-1 blends: (a) P3HT(R); (b) $W_{P3HT-1} = 0.86$; (c) P3HT-1; (d) $W_{P3HT-1} = 0.25$.

less compact. So the free volume fraction required for the glass transition (0.25) is easily achieved, and hence T_g of P3OT(R) is lesser than that of P3HT(R).[26,27]

The β transition temperature of P3OT(R) is increased by 9 °C more than that of P3HT(R) because larger side-chain length requires a greater energy (i.e., a higher temperature) for the onset of its motion. Now in the P3HT(R)/P3OT(R) blend, at the composition $W_{P3OT(R)} = 0.20$, single T_g and T_β are observed at 4.4 and −114.2 °C, respectively, indicating the compatibility in the melt state. In the miscible blends, T_g values are usually intermediate of the components values,[27,28] but the decrease in T_β compared to that of the lower value of the components is really interesting. It signifies that at this composition the side chains can easily move than those in the pure components. No definite reason is known, and it might be proposed that the hexyl and octyl groups are not as intercalated as in their ideal mixture. This is supported from Figure 7b, where there is a negative deviation of lamellar spacing at this composition. It may therefore be argued that here the side chains are somewhat squeezed and that the dispersive force of attraction between them is low as mentioned earlier. This is also supported from Table 2, where at lower lamellar thickness values the side chains become squeezed for the P3OT(R)/P3HT(R) system. As a result, they can move easily, and T_β is lower.

TABLE 2: Side-Chain Lengths for Different Interchain Lamella Distances of P3HT and P3OT Systems (Calculated from the MMX Program)

P3OT/P3HT			P3OT	
interchain lamellar distance (Å)	avg octyl chain length (Å)	avg hexyl chain length (Å)	interchain lamellar distance (Å)	avg octyl chain length (Å)
21.571	9.985	7.469	20.761	9.892
19.781	10.050	7.542	20.097	10.028
18.633	10.050	7.556	18.434	10.044
17.855	10.028	7.556	18.237	10.028
16.974	10.024	7.558	18.048	10.028
16.126	9.942	7.556		

In the blend of composition $W_{P3OT\ (R)} = 0.86$, there are two distinct T_g values (−9.4 and 25.3 °C) and two distinct T_β values (−101.1 and −78.2 °C), indicating that they are immiscible in the melting state.[3,28] So immiscibility in the melting state of the blend can be attributed as the cause of the biphasic nature of the equilibrium phase diagram. It is noteworthy that in the biphasic regions one phase shows exactly same T_β value as that of the lower T_β component and the other phase shows an increased T_β value than that of the higher T_β component by 14 °C. Probable explanation of the increased T_β value may be attributed from the lamellar spacing data of P3OT(R)-rich phase, which is 0.5 Å lower than that of P3OT(R) (Figure 7a). As a result, the octyl groups become more interdigited with each other. Consequently, the cohesive force between the side chains is larger than that in pure P3OT(R), and it requires higher temperature for the onset of the side-chain motion. From Table 2, it is clear that the P3OT lamella having of 20.76-Å length has the lowest side chain length and it increased by 0.136 Å by interdigitation of 0.66 Å. The increase in side-chain length increases the dispersion interaction of the side chains.

In the P3HT(R)/P3HT-1 system, the results are very similar to the P3HT(R)/P3OT(R) system. P3HT-1 has lower T_g and T_β values (1.8 and −112.9 °C) than those of P3HT(R) (20.3 and −101.2 °C). The two P3HTs differ by 17 mol % H−T regioregularity. As T_g of P3HT-1 is lower by 18 °C than that of P3HT(R), it indicates that irregular chains are more flexible than regular chains as proposed earlier and hence the segmental motion start at lower temperature. Again it was observed earlier from WAXS study that P3HT-1 did not exhibit any lamellar structure,[1] so the hexyl chains are not interdigitated, causing the absence of dispersion force in the hexyl groups. Consequently the onset of side-chain movement would occur at lower temperatures than that of P3HT(R). This is found to be true as P3HT-1 exhibits a T_β value at −112.9 °C. In the blend of composition $W_{P3HT-1} = 0.25$, there is a single T_g value (20.0 °C), indicating the miscibility of the components. The T_β value is also single (−103.9 °C) and is intermediate of the component values. But at the blend $W_{P3HT-1} = 0.86$, both the T_g and T_β values show doublet values, indicating that they are immiscible. The T_g values are close to those of the component values, but one T_β value is higher than that of the higher component value. The reason is probably similar to the earlier system because P3HT(R) induces P3HT-1 to form lamella,[1] and as a result, a cohesive force is developed between the interdigited hexyl groups. This results in a higher T_β value as some more energy is required to overcome the cohesive force before the onset of side chain movement. Thus the DMA results clearly indicate

that P3HT(R)/P3HT-1 ($W_{P3HT-1} = 0.86$) is phase separated in the liquid state, and this is the reason for the biphasic nature of the equilibrium phase diagram.

Conclusion

P3ATs produce equilibrium cocrystals depending on the difference of H−T concentration and alkyl chain length. The equilibrium phase diagram of P3AT cocrystals are of three different types indicating (i) weak interaction for the P3OT-(R)/P3HT-2 system, (ii) ideal mixing in P3HT-1/P3HT-2 and P3HT(R)/P3HT-2 blend, and (iii) partial miscible behavior at certain compositions of P3HT(R)/P3HT-1 and P3HT(R)/P3OT-(R) blends. The cause of the biphasic nature in the phase diagram has been found to be liquid−liquid-phase separation of the melting phase at these compositions. Both T_g and T_β values showed doublet values in the phase-separated blends, but in the miscible blends, T_g is intermediate though T_β is lower than the average value of the components. In the biphasic blend, one T_β is almost same as that of the lower component value, but the other is higher than that of the higher component value.

Acknowledgment. We gratefully acknowledge IFCPAR Grant No. 2808-2 for DMA measurements. Also we acknowledge CSIR, New Delhi (Grant No. 1655/00/EMR.II) for financial support.

Supporting Information Available: Molecular models of P3OT−P3HT and P3OT. This material is available free of charge via the Internet at http://pubs.acs.org.

References and Notes

(1) Pal, S.; Nandi, A. K. *Macromolecules* **2003**, *36*, 8426.
(2) Tanaka, H.; Lovinger, A. J.; Davis, D. D. *J. Polym. Sci* **1990**, *B28*, 2183.
(3) Guerra, G.; Karasz, F. E.; MacKnight, W. J. *Macromolecules* **1986**, *19*, 1935.
(4) Hill, M. J.; Barham, P. J.; Keller, A. *Polymer* **1992**, *33*, 2530.
(5) Natta, G.; Allegra, G.; Bassi, I. W.; Sianesi, D.; Caporiecio, G.; Torti, E. *J. Polym. Sci. A* **1965**, *3*, 4263.
(6) Datta, J.; Nandi, A. K. *Polymer* **1996**, *37*, 5179.
(7) Alamo, R. G.; Londono, J. D.; Mandelkern, L.; Stehling, F. C.; Wignall, G. D. *Macromolecules* **1994**, *27*, 411.
(8) Tashiro, K.; Izuchi, M.; Kobayashi, M.; Stein, R. S. *Macromolecules* **1994**, *27*, 1221.
(9) Runt, J.; Jin, L.; Talibuddin, S. *Macromolecules* **1995**, *28*, 2781.
(10) Kamiya, H.; Sakuri, M.; Inoue, Y.; Chugo, R. *Macromolecules* **1991**, *24*, 3888.
(11) Jeong, Y. G.; Jo, W. H.; Lee, S. C. *Macromolecules* **2000**, *33*, 9705.
(12) Tompa, H. *Polymer Solutions*; Butterworth: London, 1956.
(13) McCullough, R. D.; Ewbank, P. C. In *Handbook of Conducting polymers*, 2nd ed.; Skotheim, T. A., Elsenbaumer, R. L., Renolds, J. R., Eds.; Marcel Dekker: New York, 1998; p 225.
(14) Park, K. C.; Levon, K. *Macromolecules* **1997**, *30*, 3175.
(15) Prosa, T. J.; Winokur, M. J.; McCullough, R. D. *Macromolecules* **1996**, *29*, 3654.
(16) Amou, S.; Haba., O.; Shiroto, K.; Hayakawa, T.; Ueda, M.; Takeuchi, K.; Asai, M. *J. Polym. Sci., Polym. Chem.* **1999**, *37*, 1943.
(17) Gajewski, K. E.; Gillberr, M. H. In *Advances in Molecular Modelling*; Liotta, D., Ed; Jai Press: Greenerick, CT, 1990; Vol. 2.
(18) Hoffman, J. D.; Davis, G. T.; Lauritzen, J. L. Jr., *Treatise on Solid State Chemistry*; Hannay, N. B., Ed.; Plenum Press: New York, 1976; Vol. 3, p 497.
(19) Hoffman, J. D.; Weeks, J. J. *J. Res. Natl. Bur. Stand. (U.S.)* **1962**, *66*, 13.
(20) Rim, P. B.; Runt, J. P. *Macromolecules* **1984**, *17*, 1520.
(21) Nandi, A. K.; Mandelkern, L. *J. Polym. Sci., Polym. Phys. Ed* **1991**, *29*, 1287.
(22) Maiti, P.; Nandi, A. K. *Macromolecules* **1995**, *28*, 8511.
(23) Malik, S.; Nandi, A. K. *J. Polym. Sci, Polym. Phys. Ed.* **2002**, *40*, 2073
(24) Rahman, M. H.; Nandi, A. K. *J. Polym. Sci., Part B: Polym. Phys.* **2004**, *42*, 2215.
(25) Ferry, J. D. *Viscoelastic Properties of Polymers*; John Wiley and Sons International: New York, 1961.
(26) Kovacs, A. J. *Adv. Polym. Sci.* **1963**, *3*, 394.
(27) Nandi, A. K.; Mandal, B. M.; Bhattacharyya, S. N.; Roy, S. K. *Polym. Commun.* **1986**, *27*, 151.
(28) *Polymer Blends*; Paul, D. R., Newman, S., Eds.; Academic Press: New York, 1978; Vol. 1.